Ab initio prediction of a two-dimensional variant of the iridate IrO_2

Andriy Smolyanyuk,[1,*] Markus Aichhorn,[1] I. I. Mazin,[2] and Lilia Boeri[3,4]

[1]*Institute of Theoretical and Computational Physics, Graz University of Technology, NAWI Graz, 8010 Graz, Austria*

[2]*Code 6393, Naval Research Laboratory, Washington, DC 20375, USA*

[3]*Department of Physics, Sapienza Università di Roma, 00185 Rome, Italy*

[4]*Istituto dei Sistemi Complessi (ISC)-CNR, 00185 Rome, Italy*

(Received 4 July 2019; revised manuscript received 17 October 2019; published 9 December 2019)

We propose an insulating two-dimensional phase of IrO_2, predicted by *ab initio* evolutionary algorithms. The predicted phase is a van der Waals crystal, in which Ir forms a triangular lattice, and is energetically competitive with the metastable spinel phase, observed experimentally. Electronic structure calculations show that the magnetic properties of this phase are highly nontrivial, with an almost perfect degeneracy of 120° *Néel* and *Y*-stripe orders, and unusually soft magnetic moments. The resulting behavior, which we term *easy plane anisotropy*, is entirely different from what is realized in previously explored Kitaev honeycomb lattices. Our results thus suggest that IrO_2 may be an ideal candidate to realize highly unusual magnetic properties.

DOI: 10.1103/PhysRevB.100.235114

I. INTRODUCTION

Two-dimensional materials represent an ideal platform to investigate exotic physical phenomena, such as charge-density wave, superconductivity, topological order, etc., and have a wide range of applicability in different fields, ranging from coating to two-dimensional (2D) electronics [1–3]. The best known systems are usually obtained by mechanical exfoliation of bulk van der Waals crystals, such as graphene [4] (graphite), *h*-BN [5], transition metal dicalchogenides (TMDCs) [6], or MXenes [7].

Besides investigating the properties of materials derived from known bulk phases, an emerging trend in the field of 2D materials is to use computational methods in order to discover, predict, and characterize completely new structures. For example, Ref. [8] investigated the stability of single-layer MX_2 transition metal oxides and dichalcogenides in honeycomblike structures, data mining of structures listed in various databases was employed to filter out possible 2D materials [9], high-throughput computations were used to determine possible exfoliation of experimentally known compounds [10], and evolutionary algorithms were used to predict new 2D materials [11,12].

Most 2D materials known up to now are nonmagnetic metals, semiconductors, or insulators. The Mermin-Wagner theorem postulates that magnetic order is forbidden in the two-dimensional Heisenberg model at finite temperature [13]. However, recently magnetism in 2D van der Waals crystals was discovered [14,15], showing that long-range magnetic order is indeed possible in 2D systems, since magnetic anisotropy removes the restriction coming from the Mermin-Wagner theorem. This opens the road to the discovery of many other 2D magnetic systems.

In this work, using evolutionary crystal structure prediction, we identify a hypothetical 2D phase of IrO_2, which is a purely 2D system with strongly anisotropic magnetic interactions, including, but not limited to, the Kitaev interaction. The Kitaev model [16] has been studied theoretically by several authors [17–19]. Experimental realizations have been proposed in several systems, such as, for instance, Na_2IrO_3, α-Li_2IrO_3, Li_2RhO_3, and α-$RuCl_3$ [20]. The initial proposal by Jackeli *et al.* [21] was to realize the Kitaev model on the honeycomb lattice, also noting the possibility to apply the model to the triangular lattice formed by edge-shared IrO_6 octahedra, typical, for instance, in layered ABO_2 compounds where *A* and *B* are alkali and transition metal ions, respectively. In all the above proposals, the transition metal sublattice is effectively embedded in a three-dimensional framework, while in 2D IrO_2 the Kitaev physics may be realized even on a single monolayer.

Once realized on the triangular lattice, the Kitaev model and more complicated variants, such as the Heisenberg-Kitaev model with possible extensions by additional symmetry-allowed anisotropies, show rich phase diagrams. Apart from conventional ordered phases, they include exotic phases with nematic order, $\mathbb{Z}_2$-vortex crystal phases [22–24], and the quantum spin-liquid state [25,26]. Another interesting finding is that quantum order-by-disorder effects are present in the Kitaev model on the triangular lattice that lead to a selection of the easy axes, which in turn reduces the degeneracy of the ground state [27].

Using first-principles calculations based on density functional theory (DFT), we find that our new 2D-IrO_2 structure is dynamically stable, van der Waals bound (i.e., easy to exfoliate), and most intriguingly, exhibits a highly unusual discrete magnetic frustration, namely, a 120° noncollinear structure with a particular spin orientation with respect to crystallographic axes is essentially degenerate with a stripe order, again with a specific spin orientation. This degeneracy cannot be reproduced by a short-range bilinear coupling, whether isotropic or anisotropic, and may have ramifications far beyond the scope of this paper.

*andriysmolyanyuk@gmail.com

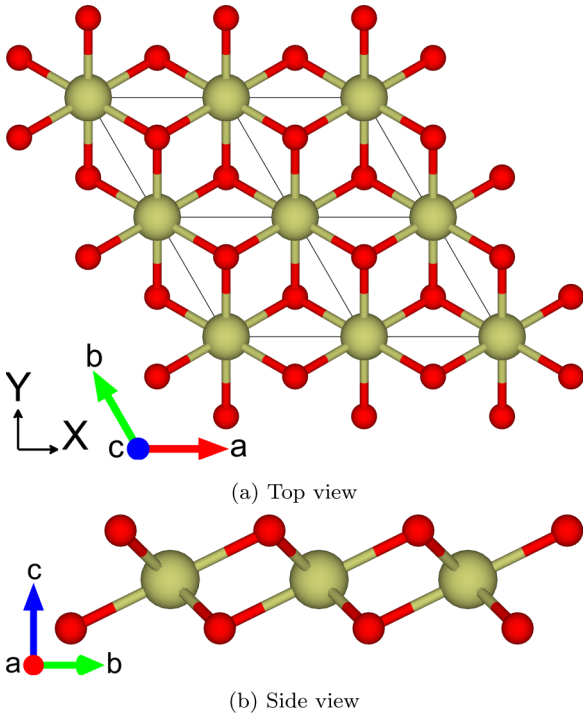

(a) Top view

(b) Side view

FIG. 1. $1T$ IrO_2 polytype crystal structure: dark-gray (red) are oxygen atoms, light-gray (green) are iridium atoms; (a) top view, (b) side view. The X, Y axes indicate the global (XYZ) coordinate system.

Even more unusual is the softness of the Ir magnetic moment, which can only have a full magnetization consistent with $j_{\text{eff}} = 1/2$ when the moments lie in the plane. If rotated away from the plane, the moment rapidly collapses to essentially zero. This is in some sense similar to the popular XY model, but this similarity is misleading: in the XY model magnetic moments are strictly restricted within the plane, while in our case they can be rotated away, but their amplitude rapidly decreases with the angle; such excitations, impossible in the XY model, are allowed here, so that the system would have different spin dynamics, different response to magnetic field, and even different thermodynamics. Such a system is qualitatively different from usually studied 2D materials and represents an intriguing and unusual class of magnetic models.

Our paper is structured as follows: In Sec. II we introduce the $1T$ IrO_2 structure, and study its energetics and structural stability; in Sec. III we describe the effect of crystal field, spin-orbit coupling, and local electronic correlations on the electronic structure; in the next section, Sec. IV, we discuss the unusual magnetic properties predicted by DFT, and the relevance of different model Hamiltonians to our results. Finally, in the Appendix we describe the details of the evolutionary search that led us to discover 2D IrO_2, and provide the computational details used for all our calculations.

II. CRYSTAL STRUCTURE AND STRUCTURAL STABILITY

The crystal structure of 2D IrO_2 is shown in Fig. 1; it is analogous to the $1T$ polytype of many TMDCs. In this structure, iridium is arranged on a triangular lattice, at the centers of O_6 octahedra, with slight trigonal distortion (negative) (see the structure parameters in Table I).

TABLE I. 2D-IrO_2 crystal structure: space group no. 136 ($P\bar{3}2/m1$); the lattice parameters are $a = b = 3.16$ Å, $\alpha = \beta = 90^\circ$, $\gamma = 120^\circ$ and a sufficiently large vacuum layer was inserted.

Atom	Site	x	y	z
Ir	$1a$	0	0	0
O	$2d$	$\frac{1}{3}$	$\frac{2}{3}$	0.073

Our $1T$ IrO_2 structure, as detailed in the Appendix, was identified almost accidentally through a sequence of several evolutionary crystal structure runs, and appears to be a very stable local minimum of the energy landscape of IrO_2, where the dominant minima are the two known bulk phases, with rutile [28] and spinel [29] structures. To the best of our knowledge, this is the first time that a 2D structure is predicted for IrO_2; however, 2D structures that are markedly different from the bulk structures have been predicted for other binary oxides, such as SiO_2 and TiO_2 [30,31].

Table II lists the energetics of different IrO_2 phases. The stabilization energy of $1T$ IrO_2 (∼240 meV/atom), compared to the bulk rutile phase, is in the same ballpark as what is found for many compounds that exhibit competing layered and bulk phases, such as diamond and graphite [32], h and cubic BN [33], etc. Indeed, $1T$ IrO_2 appears to be not only more stable energetically than other 2D polytypes [34], but also compared to surface terminations of the rutile ground-state structure and to the first metastable bulk phase, i.e., spinel; thus, it could be very likely synthesized experimentally.

According to our calculation, $1T$ IrO_2 is stable in both monolayer and bulk form; in fact, our calculations suggest that the latter becomes the ground state at ∼160 GPa, overcoming the two 3D bulk structures. This bulk layered phase is a van der Waals crystal, as can be demonstrated by optimizing with and one without a van der Waals correction (we used the one from Ref. [35], but it is well known that alternative choices yield similar results). We found that the interlayer distance in the two cases differs by 3.3 Å (9.65 vs 6.35 Å), which is larger than for representative transition metal dichalcogenides ($7.4 - 6.0 = 1.4$ Å for MoS_2, $6.9 - 6.0 = 0.9$ Å for $NbSe_2$), and similar to that in graphite ($8.8 - 6.6 = 2.2$ Å) [36]. This means that, once synthesized, $1T$ IrO_2 will be easily exfoliable.

After the structure was determined, we checked its dynamical stability by calculating the phonon dispersion. We used a

TABLE II. Comparison of energies of various 2D-IrO_2 phases (nonmagnetic calculations including spin-orbit coupling).

Name	Energy/atom (meV)
Rutile (bulk)	0
$1T$	237
Spinel (bulk)	266
Rutile (001)	326
Rutile (110)	385
$1H$	621

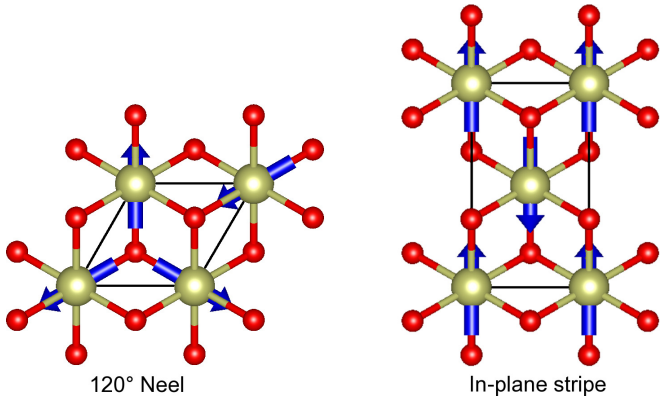

FIG. 2. The two nearly degenerate $1T$ IrO_2 magnetic configurations, which are lowest in energy. The arrows show the directions of the spin magnetic moments on the Ir atoms in the XY plane.

finite displacement method as implemented in the PHONOPY package [37], using a $2 \times 2 \times 1$ supercell. Under realistic conditions, i.e., including spin-orbit coupling (SOC), strong correlations, and magnetism (see next paragraph), $1T$ IrO_2 is dynamically stable.

III. ELECTRONIC STRUCTURE

Ir^{4+} has one unpaired electron so one expects the ground state to be magnetic. As commonly done for Ir^{4+} compounds, we have included electronic correlations using the GGA + U method with $U - J = 2$ eV, a typical value for such systems [38–40].

We find two completely different magnetic ground states, degenerate on the level of computational accuracy of $\lesssim 1$ meV/Ir. These two configurations are the 120°-Néel orientation and an *in-plane stripe* order with magnetic moments directed along the global Y axis, which we will denote as Y *stripes*, as shown in Fig. 2. The 120°-Neel configuration is formed by three sublattices oriented at a 120° angle with respect to each other, and the Y stripes configuration is formed by antiferromagnetically coupled rows of collinear spins lying in the layer's plane. Our calculations show no qualitative changes in the properties of $1T$ IrO_2 for $1.3 < U - J < 4.0$ eV, and the above-mentioned degeneracy of magnetic phases is observed in this region.

In both cases the system forms a weak Mott-Hubbard insulator; using $U - J = 2.0$ eV, the band gap for the 120°-Néel structure is 0.42 eV and for the Y stripes it is 0.24 eV.

The origin of the gap is the same as in other Ir^{4+} iridates. The t_{2g} splits into a doublet and a quartet, reminiscent of the $j_{\text{eff}} = 1/2$ and $j_{\text{eff}} = 3/2$ spin-orbit driven splitting of a t_{2g} level. The doublet forms a narrow half-filled band that can be easily split by a moderate Hubbard interaction [42]. As one can see in the lower panel of Fig. 3, already for $U = 0$ the exchange splitting is trying to open the gap, but it is too weak. Adding a finite U eventually opens up a gap.

IV. MAGNETIC STRUCTURE

Magnetic interactions are strongly anisotropic (see Table III and top panel of Fig. 4). For rotations of the stripe order out of the XY plane the minimum of the energy corresponds to the in-plane direction, while for rotations in the XY plane the Y direction, orthogonal to an Ir-Ir bond, is energetically more favorable. Importantly, as Fig. 4 shows, as magnetic moments are rotated away from the XY plane by more than approximately 15°, they collapse from 0.4–0.5μ_B to 0.1μ_B or less (numbers are given for spin moments; the total moments drop from about 1.0 to 0.2–0.25μ_B).

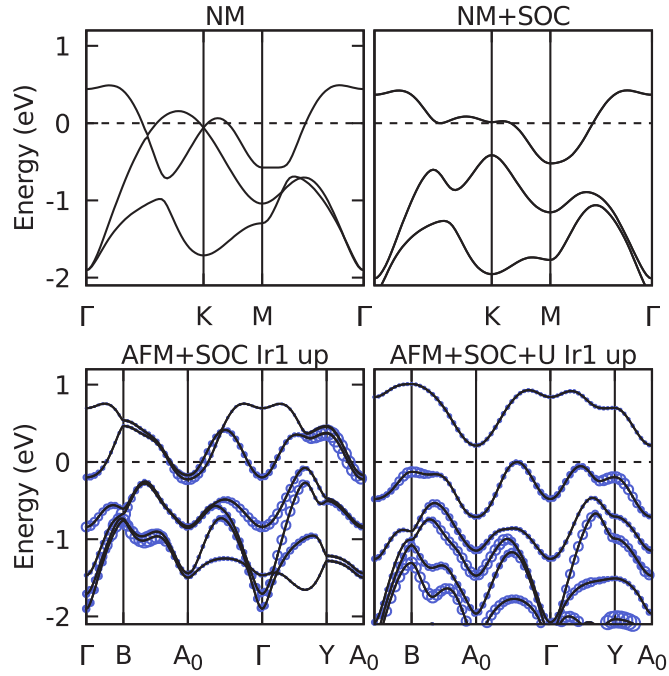

FIG. 3. Band structure of $1T$ IrO_2 states for nonmagnetic IrO_2 with and without spin-orbit coupling (top panel), and the Y-stripe AFM configuration with SOC and with or without $U = 2.7$ eV (bottom panel). The bottom panels show the projection on the single Ir spin-up states ($m_s = \frac{1}{2}$ states) with quantization axis in the Y direction. Calculations are done with WIEN2K [41]. The high-symmetry k points are (upper panel) $\Gamma(0,0,0)$, $K(\frac{1}{3},\frac{1}{3},0)$, $M(\frac{1}{2},0,0)$ for trigonal cell ($a = b = 3.16$ Å, $\alpha = \beta = 90°$, $\gamma = 120°$) and (bottom panel) $\Gamma(0,0,0)$, $B = (\frac{1}{2},0,0)$, $Y = (0,\frac{1}{2},0)$, $A_0 = (\frac{1}{2},\frac{1}{2},0)$ for monoclinic supercell ($a = 3.16$ Å, $b = 5.47$ Å, $\alpha = \beta = \gamma = 90°$).

TABLE III. Energy and absolute values of the spin and orbital magnetic moments for different magnetic phases. The direction of the magnetic moment is denoted in the global coordinate system; the last column shows energies (per formula unit) estimated using the in-plane Hamiltonian Eq. (2) with the parameters from Table IV. Note that the energy fits are not applicable to out-of-plane directions, lines 3 and 7.

Name	Energy/f.u. (meV)	m_s (μ_B)	m_l (μ_B)	E_{fit} (meV)
120 Néel	0	0.40	0.50	4
Y stripe	0	0.43	0.55	0
Z stripe	9	0.09	0.11	
X stripe	16	0.35	0.50	16
Y FM	34	0.47	0.61	35
X FM	34	0.47	0.61	35
Z FM	49	0.09	0.16	

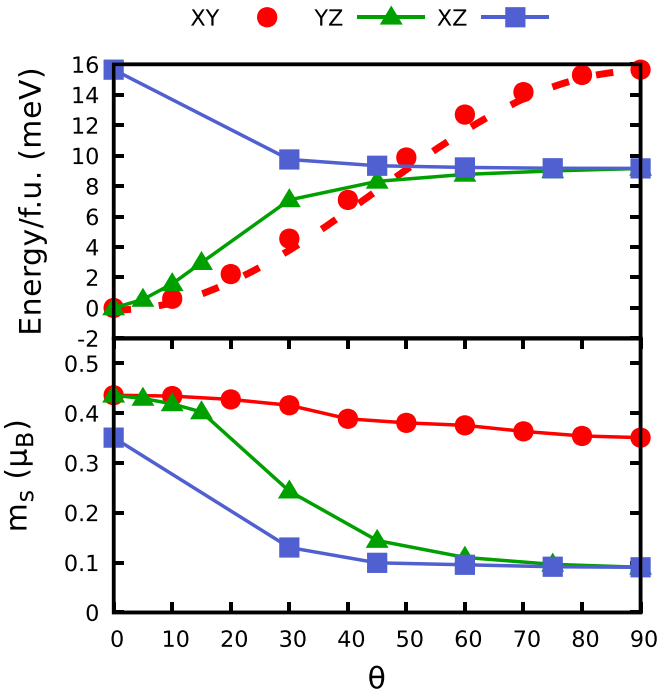

FIG. 4. Dependence of the energy (top panel) and the spin magnetic moment on the Ir site (bottom panel) on the rotation angle for stripe order, with spins rotating in the XY (circles), YZ (triangles), and XZ (squares) planes. The dashed line is the fit of energy of XY rotations to the model defined by Eq. (2). For rotations in the XY plane, θ is the in-plane rotation angle, and $\theta = 0$ corresponds to the Y direction; for rotations in the YZ and XZ planes, the angle θ is the out-of-plane rotation angle, with $\theta = 0$ indicating the in-plane direction. Solid lines are meant as a guide to the eye.

It has become customary to use the following anisotropic exchange model, often referred to it as an extended Heisenberg-Kitaev (EHK) Hamiltonian, for describing magnetic interactions in iridates. It can be conveniently written using the form suggested in Refs. [18,21,43]:

$$H = \sum_{\langle ij \rangle} J\left(S_i^x S_j^x + S_i^y S_j^y + \Delta S_i^z S_j^z\right) + 2J_{\pm\pm}\left[\left(S_i^x S_j^x - S_i^y S_j^y\right)c_\alpha - \left(S_i^x S_j^y + S_i^y S_j^x\right)s_\alpha\right] + J_{z\pm}\left[\left(S_i^y S_j^z + S_i^z S_j^y\right)c_\alpha - \left(S_i^x S_j^z + S_i^z S_j^x\right)s_\alpha\right]. \quad (1)$$

The sum above is over nearest-neighboring sites i and j; $c_\alpha = \cos\varphi_\alpha$ and $s_\alpha = \sin\varphi_\alpha$, where $\varphi_\alpha = \{0, \frac{2\pi}{3}, -\frac{2\pi}{3}\}$ is the bond angle between the direction of the ij bond and the X axis.

An interesting issue, not always brought to light, is the physical meaning of the operators S here. Given a single (Kramers-degenerate, in absence of a magnetic field) band, separated from the rest of the t_{2g} manifold, it is always possible to assign to it a pseudospin quantum number that would have the same property as a spin-1/2 operator. The beauty of Eq. (1), as applied to materials such as Na_2IrO_3 or $RuCl_3$, is that this pseudospin has a direct, simple and physically transparent interpretation in terms of $j_{\rm eff} = 1/2$ states. The latter have the spin and orbital moment collinear, adding up to $M = M_s + M_l = 1\mu_B$, so that the direction of S coincides with the directions of M and M_s, and the g factor is isotropic and equal to 2. This is, approximately, the case in Na_2IrO_3, but as we will discuss later, not entirely so in our compound.

Exchange parameters in Eq. (1) can also be rewritten in the notations of Ref. [18] as $J_{\pm\pm} = \frac{1}{6}(2\Gamma' - 2\Gamma - K)$, $J_{z\pm} = \frac{\sqrt{2}}{3}(K - \Gamma + \Gamma')$, $J\Delta = \frac{1}{3}(3\widetilde{J} + K + 2\Gamma + 4\Gamma')$ (since the same symbol J is used in Refs. [18] and [43] we substitute it by $\widetilde{J}$ when we talk about notations from Ref. [18]). While the easy-plane anisotropy is not affected by pure Kitaev interactions, it is affected by the non-Kitaev terms Γ and Γ'. J is the bond-independent isotropic magnetic interaction term, $J_{\pm\pm}$ (anisotropy in the XY plane) and $J_{z\pm}$ (anisotropy in the YZ plane) are the bond-dependent anisotropic terms, and Δ is what is usually called the Ising exchange. For collinear spins, the contribution of $J_{z\pm}$ cancels out, and an easy-plane anisotropy is solely determined by Δ; $\Delta > 1$ corresponds to an easy Z axis, and $\Delta < 1$ corresponds to an XY easy-plane anisotropy. However, for other magnetic configurations an easy-plane vs easy-axis anisotropy involves also $J_{z\pm}$, whereas $J_{\pm\pm}$ produces an anisotropy within the XY plane.

The easy-plane anisotropy that we see in the calculations is, on the first glance, an indication of a sizable Δ with $J_{z\pm} \to 0$, since nonzero $J_{z\pm}$ favors out-of-plane direction. However, a closer look reveals that in our case the most important contribution to the anisotropy does not come from Δ, but from the near collapse of the magnetic moment for out-of-plane directions (see the bottom panel of Fig. 4). This observation is in direct contradiction with the $j_{\rm eff} = 1/2$ description, and can only be reconciled with a description in terms of pseudospins if a highly anisotropic and/or strongly nondiagonal g tensor is assumed. Direct inspection of the band structure in a collapsed moment state indicates that the split-off hole band changes its spin polarization as a function of k and the latter integrates to nearly zero. This is the effect of strong hybridization of the hole band with other electronic states that prevents us from describing it as a nearly pure $j_{\rm eff} = 1/2$ state. Not having access to the pseudospin direction (note that in either experiment or DFT calculations only the magnetic moments are observed, and the pseudospins, being a mathematical construct, are not directly accessible) we cannot therefore evaluate the parameters of the Hamiltonian Eq. (1) for the situations where the actual magnetic moments collapse.

On the other hand, as long as only in-plane spins are considered, the pseudospin description is not that far from the $j_{\rm eff} = \frac{1}{2}$ description; the calculated spin and orbital moments are indeed parallel to each other [and this direction can be taken as the direction of S in Eq. (1)]. They add up to numbers consistent with $M = 1\mu_B$ (with a reasonable hybridization reduction), and thus can be used in Eq. (1) in a meaningful way:

$$H = \sum_{\langle ij \rangle} J\left(S_i^x S_j^x + S_i^y S_j^y\right) + 2J_{\pm\pm}\left[\left(S_i^x S_j^x - S_i^y S_j^y\right)c_\alpha - \left(S_i^x S_j^y + S_i^y S_j^x\right)s_\alpha\right]. \quad (2)$$

The classical per-site energies of the phases with magnetization directions in the XY plane, namely the 120° order,

TABLE IV. Parameters of the restricted Heisenberg-Kitaev Hamiltonian Eq. (2), obtained by a least-square fit.

J (meV)	$J_{\pm\pm}$ (meV)	E_0 (meV)
6.7 ± 0.4	2.0 ± 0.2	14.4 ± 0.5

rotations of the stripe order in the XY plane, and an in-plane FM order (see Fig. 4 and Table III) are

$$E_{120} = E_0 - \tfrac{3}{2}J, \tag{3}$$

$$E_{XY}^{\text{Stripe}} = E_0 - J - 4J_{\pm\pm}\cos 2\theta, \tag{4}$$

$$E_{\text{FM}} = E_0 + 3J, \tag{5}$$

where $\theta = 0$ corresponds to the Y direction. We want to note that the energy of in-plane 120° order does not change upon the rotation around Z axis. However, out-of-plane variants of 120° order are higher in energy.

The least-squares fit of J, $J_{\pm\pm}$, and E_0 to the available data is shown in Table IV, while the energies predicted by the fitted model for different magnetic configurations are shown in the last column of Table III (E_{fit}). The agreement in this case is quite good, indicating that the in-plane restricted model is a rather good match for DFT energies.

The anisotropic $J_{\pm\pm}$ term is only three times smaller than the isotropic J term, emphasizing strong *in-plane* anisotropy. This is in addition to the above-mentioned nontrivial anisotropy stemming from the softness of magnetic moments. The degeneracy of the 120° Néel and the Y-stripe configurations is only reproduced within 4 meV, while in the calculations the two configurations are degenerate within a fraction of meV. Such an accidental discontinuous degeneracy, a consequence of the intrinsic magnetic frustration, adds a further exciting aspect to the unusual spin dynamics of this system.

V. CONCLUSIONS

We predicted a hypothetical insulating layered phase of IrO_2 with a triangular Ir^{4+} lattice—1T IrO_2. We show that it is likely to be a very stable phase, albeit not the most stable phase. The bonding between the layers is very weak, so monolayers could be easily obtained by exfoliation. The Ir^{4+} ions are in an (approximately) $j_{\text{eff}} = 1/2$ state, as are most other Ir^{4+} iridates, too. Our *ab initio* calculations reveal several highly unusual aspects of magnetism in this system: (i) a nontrivial accidental degeneracy of the magnetic ground state: the 120° *Néel* orientation and the Y stripe (in-plane orientation perpendicular to the Ir-Ir bonds) are degenerate down to 1 meV/atom; (ii) a strong magnetic anisotropy even within the hexagonal plane, a reflection of strong bond-dependent magnetic exchange interactions; (iii) finally, the calculated moments are exceptionally soft in the sense that they essentially disappear if forced to tilt away from the plane. This behavior can be called an "easy-plane anisotropy," but this anisotropy is physically very distinct from the "conventional" easy-plane behavior, provided by either single-site or exchange anisotropy. Thus, despite the same geometry as honeycomb iridates, in 1T IrO_2 Kitaev interaction does not strongly dominate the magnetic physics. This system is entirely different from previously explored Kitaev honeycomb lattices, and promises nontrivial and yet unexplored magnetic properties.

ACKNOWLEDGMENTS

We acknowledge funding from the Austrian Science Fund FWF through SFB ViCoM, Project No. F04115, and START program Y746, and computational resources from the VSC3 of the Vienna University of Technology and HPC TU Graz. I.I.M. acknowledges support by ONR through the NRL basic research program and Sapienza University of Rome through Bando Professori Visitatori 2018.

APPENDIX: COMPUTATIONAL DETAILS

1. Details of the crystal structure search

The proposed structure was identified through a sequence of several evolutionary crystal structure runs, performed with the USPEX package [44–46] employing four-step structural relaxation. First, in an unbiased 3D structure search, we realized that metastable 2D structures of IrO_2, with stabilization energies of 200 meV, coexisted with the known bulk structures. For a further refinement we repeated the search with different accuracies, but limiting our search to 2D structures. This yielded 1T as the most stable polytype [34], also compared to (001) and (110) cuts of the rutile surface; see Table II.

2. Details of DFT calculation

To calculate the total energies and perform structural optimization we used density functional theory (DFT) in the generalized gradient approximation (GGA) with the Perdew-Burke-Ernzerhof functional [47,48] as implemented in the VASP package [49–52] using the projector augmented wave method (PAW) [53,54].

For the postprocessing of the results from the evolutionary search and calculation of properties the energy cutoff was set to 600 eV, and a Γ-centered Monkhorst-Pack grid [55,56] with the reciprocal-space resolution of 0.023 2π Å^{-1} was used. For the magnetic calculations the Wigner-Seitz radius was set to 1.423 and 0.9 Å for Ir and O atoms respectively; the penalty term λ for constrained magnetic calculations was set to the value 10.

The band structure plots shown in Fig. 3 were obtained with WIEN2K [57]. Due to different implementations of the GGA + U method in VASP and WIEN2K, the value of U is not directly transferable between the two codes. For that reason, we had to use a slightly larger value of $U = 2.7$ eV when using WIEN2K. This value yields a similar gap as for VASP calculations with $U = 2.0$ eV. For the WIEN2K calculations we used a $16 \times 16 \times 1$ k mesh, defined on a Γ-centered point grid [58].

[1] K. S. Novoselov, A. Mishchenko, A. Carvalho, and A. H. C. Neto, Science **353**, aac9439 (2016).

[2] J. Wang, F. Ma, and M. Sun, RSC Adv. **7**, 16801 (2017).

[3] G. Fiori, F. Bonaccorso, G. Iannaccone, T. Palacios, D. Neumaier, A. Seabaugh, S. K. Banerjee, and L. Colombo, Nat. Nanotechnol. **9**, 768 (2014).

[4] K. S. Novoselov, A. K. Geim, S. V. Morozov, D. Jiang, Y. Zhang, S. V. Dubonos, I. V. Grigorieva, and A. A. Firsov, Science **306**, 666 (2004).

[5] A. Nagashima, N. Tejima, Y. Gamou, T. Kawai, and C. Oshima, Phys. Rev. Lett. **75**, 3918 (1995).

[6] M. Bosi, RSC Adv. **5**, 75500 (2015).

[7] M. Khazaei, A. Ranjbar, M. Arai, T. Sasaki, and S. Yunoki, J. Mater. Chem. C **5**, 2488 (2017).

[8] C. Ataca, H. Şahin, and S. Ciraci, J. Phys. Chem. C **116**, 8983 (2012).

[9] S. Lebègue, T. Björkman, M. Klintenberg, R. M. Nieminen, and O. Eriksson, Phys. Rev. X **3**, 031002 (2013).

[10] N. Mounet, M. Gibertini, P. Schwaller, D. Campi, A. Merkys, A. Marrazzo, T. Sohier, I. E. Castelli, A. Cepellotti, G. Pizzi, and N. Marzari, Nat. Nanotechnol. **13**, 246 (2018).

[11] A. R. Oganov, J. Chen, C. Gatti, Y. Ma, Y. Ma, C. W. Glass, Z. Liu, T. Yu, O. O. Kurakevych, and V. L. Solozhenko, Nature (London) **457**, 863 (2009).

[12] X.-F. Zhou, X. Dong, A. R. Oganov, Q. Zhu, Y. Tian, and H.-T. Wang, Phys. Rev. Lett. **112**, 085502 (2014).

[13] N. D. Mermin and H. Wagner, Phys. Rev. Lett. **17**, 1133 (1966).

[14] B. Huang, G. Clark, E. Navarro-Moratalla, D. R. Klein, R. Cheng, K. L. Seyler, D. Zhong, E. Schmidgall, M. A. McGuire, D. H. Cobden, W. Yao, D. Xiao, P. Jarillo-Herrero, and X. Xu, Nature (London) **546**, 270 (2017).

[15] C. Gong, L. Li, Z. Li, H. Ji, A. Stern, Y. Xia, T. Cao, W. Bao, C. Wang, Y. Wang, Z. Q. Qiu, R. J. Cava, S. G. Louie, J. Xia, and X. Zhang, Nature (London) **546**, 265 (2017).

[16] A. Kitaev, Ann. Phys. **321**, 2 (2006), January Special Issue.

[17] I. Kimchi and A. Vishwanath, Phys. Rev. B **89**, 014414 (2014).

[18] J. Chaloupka and G. Khaliullin, Phys. Rev. B **92**, 024413 (2015).

[19] J. Chaloupka and G. Khaliullin, Phys. Rev. B **94**, 064435 (2016).

[20] S. M. Winter, A. A. Tsirlin, M. Daghofer, J. van den Brink, Y. Singh, P. Gegenwart, and R. Valenti, J. Phys.: Condens. Matter **29**, 493002 (2017).

[21] G. Jackeli and G. Khaliullin, Phys. Rev. Lett. **102**, 017205 (2009).

[22] M. Becker, M. Hermanns, B. Bauer, M. Garst, and S. Trebst, Phys. Rev. B **91**, 155135 (2015).

[23] A. Catuneanu, J. G. Rau, H.-S. Kim, and H.-Y. Kee, Phys. Rev. B **92**, 165108 (2015).

[24] I. Rousochatzakis, U. K. Rössler, J. van den Brink, and M. Daghofer, Phys. Rev. B **93**, 104417 (2016).

[25] Y. Li, G. Chen, W. Tong, L. Pi, J. Liu, Z. Yang, X. Wang, and Q. Zhang, Phys. Rev. Lett. **115**, 167203 (2015).

[26] Y.-D. Li, X. Wang, and G. Chen, Phys. Rev. B **94**, 035107 (2016).

[27] G. Jackeli and A. Avella, Phys. Rev. B **92**, 184416 (2015).

[28] V. Goldschmidt, T. Barth, D. Holmsen, G. Lunde, and W. Zachariasen, Skrifter utgitt av det Norske Videnskaps-Akademi i Oslo 1: Matematisk-Naturvidenskapelig Klasse, 1 (1926).

[29] H. Kuriyama, J. Matsuno, S. Niitaka, M. Uchida, D. Hashizume, A. Nakao, K. Sugimoto, H. Ohsumi, M. Takata, and H. Takagi, Appl. Phys. Lett. **96**, 182103 (2010).

[30] V. O. Özçelik, S. Cahangirov, and S. Ciraci, Phys. Rev. Lett. **112**, 246803 (2014).

[31] H. A. Eivari, S. A. Ghasemi, H. Tahmasbi, S. Rostami, S. Faraji, R. Rasoulkhani, S. Goedecker, and M. Amsler, Chem. Mater. **29**, 8594 (2017).

[32] H. Shin, S. Kang, J. Koo, H. Lee, J. Kim, and Y. Kwon, J. Chem. Phys. **140**, 114702 (2014).

[33] A. Janotti, S.-H. Wei, and D. J. Singh, Phys. Rev. B **64**, 174107 (2001).

[34] A. Guinier, G. B. Bokij, K. Boll-Dornberger, J. M. Cowley, S. Ďurovič, H. Jagodzinski, P. Krishna, P. M. de Wolff, B. B. Zvyagin, D. E. Cox, P. Goodman, T. Hahn, K. Kuchitsu, and S. C. Abrahams, Acta Crystallogr., Sect. A **40**, 399 (1984).

[35] A. Tkatchenko and M. Scheffler, Phys. Rev. Lett. **102**, 073005 (2009).

[36] T. Bučko, S. Lebègue, J. Hafner, and J. G. Ángyán, Phys. Rev. B **87**, 064110 (2013).

[37] A. Togo and I. Tanaka, Scr. Mater. **108**, 1 (2015).

[38] S. M. Winter, Y. Li, H. O. Jeschke, and R. Valentí, Phys. Rev. B **93**, 214431 (2016).

[39] P. Liu, S. Khmelevskyi, B. Kim, M. Marsman, D. Li, X.-Q. Chen, D. D. Sarma, G. Kresse, and C. Franchini, Phys. Rev. B **92**, 054428 (2015).

[40] K. Li, S.-L. Yu, and J.-X. Li, New J. Phys. **17**, 043032 (2015).

[41] The value of U was set to 2.7 eV (0.2 Ry) since higher U is needed to open the gap when calculations are employed by WIEN2K due to the difference between implementations (the value of U is not transferable between VASP and WIEN2K software).

[42] B. J. Kim, H. Jin, S. J. Moon, J.-Y. Kim, B.-G. Park, C. S. Leem, J. Yu, T. W. Noh, C. Kim, S.-J. Oh, J.-H. Park, V. Durairaj, G. Cao, and E. Rotenberg, Phys. Rev. Lett. **101**, 076402 (2008).

[43] P. A. Maksimov, Z. Zhu, S. R. White, and A. L. Chernyshev, Phys. Rev. X **9**, 021017 (2019).

[44] A. R. Oganov and C. W. Glass, J. Chem. Phys. **124**, 244704 (2006).

[45] A. O. Lyakhov, A. R. Oganov, H. T. Stokes, and Q. Zhu, Comput. Phys. Commun. **184**, 1172 (2013).

[46] A. R. Oganov, A. O. Lyakhov, and M. Valle, Acc. Chem. Res. **44**, 227 (2011).

[47] J. P. Perdew, K. Burke, and M. Ernzerhof, Phys. Rev. Lett. **77**, 3865 (1996).

[48] J. P. Perdew, K. Burke, and M. Ernzerhof, Phys. Rev. Lett. **78**, 1396 (1997).

[49] G. Kresse and J. Hafner, Phys. Rev. B **47**, 558 (1993).

[50] G. Kresse and J. Hafner, Phys. Rev. B **49**, 14251 (1994).

[51] G. Kresse and J. Furthmüller, Comput. Mater. Sci. **6**, 15 (1996).

[52] G. Kresse and J. Furthmüller, Phys. Rev. B **54**, 11169 (1996).

[53] G. Kresse and D. Joubert, Phys. Rev. B **59**, 1758 (1999).

[54] P. E. Blöchl, Phys. Rev. B **50**, 17953 (1994).

[55] H. J. Monkhorst and J. D. Pack, Phys. Rev. B **13**, 5188 (1976).

[56] J. D. Pack and H. J. Monkhorst, Phys. Rev. B **16**, 1748 (1977).

[57] P. Blaha, K. Schwarz, G. K. H. Madsen, D. Kvasnicka, and J. Luitz, *WIEN2K, An Augmented Plane Wave + Local Orbitals Program for Calculating Crystal Properties* (Karlheinz Schwarz, Techn. Universität Wien, Austria, 2001).

[58] P. E. Blöchl, O. Jepsen, and O. K. Andersen, Phys. Rev. B **49**, 16223 (1994).